Subsystem functionals and the missing ingredient of confinement physics in density functionals

Feng Hao,[1,*] Rickard Armiento,[2,†] and Ann E. Mattsson[1,‡]
[1]*Multiscale Dynamic Materials Modeling, MS 1322, Sandia National Laboratories, Albuquerque, New Mexico 87185-1322, USA*
[2]*Department of Materials Science and Engineering, Massachusetts Institute of Technology, Cambridge, Massachusetts 02139, USA*
(Received 19 April 2010; revised manuscript received 14 July 2010; published 3 September 2010)

The subsystem functional scheme is a promising approach recently proposed for constructing exchange-correlation density functionals. In this scheme, the physics in each part of real materials is described by mapping to a characteristic model system. The "confinement physics," an essential physical ingredient that has been left out in present functionals, is studied by employing the harmonic-oscillator (HO) gas model. By performing the potential→density and the density→exchange energy per particle mappings based on two model systems characterizing the physics in the interior (uniform electron-gas model) and surface regions (Airy gas model) of materials for the HO gases, we show that the confinement physics emerges when only the lowest subband of the HO gas is occupied by electrons. We examine the approximations of the exchange energy by several state-of-the-art functionals for the HO gas, and none of them produces adequate accuracy in the confinement dominated cases. A generic functional that incorporates the description of the confinement physics is needed.

DOI: 10.1103/PhysRevB.82.115103 PACS number(s): 71.15.Mb, 31.15.E−, 71.45.Gm

I. INTRODUCTION

In the past few decades, Kohn-Sham (KS) density-functional theory (DFT) (Refs. 1 and 2) has been tremendously successful in electronic-structure calculations for a great variety of systems, owing to its exceptional ability to provide accurate calculations while still keeping a relatively low computational cost. In DFT, the difficult part of many-body effects are reformulated into the exchange-correlation (XC) energy E_{XC}, as a functional of the ground-state electron density n. A good approximation to the universal XC energy functional is the critical prerequisite for accurate DFT-based modeling.

One area where DFT with regular, semilocal, XC functionals has been less successful is solid-state systems with highly localized states, such as bonds originating from d and f electrons as typically found in transition-metal compounds (see, e.g., Refs. 3 and 4). This problem is often discussed as one effect of the self-interaction error that originates from a surplus electrostatic term in the Hartree energy. Common XC functionals cancel much of this positive energy contribution but the remaining part artificially increases the energy of localized states and leads to overdelocalization. Many different schemes have been proposed to address the self-interaction error, some well-known examples include (i) an explicit orbital-dependent correction that removes the surplus electrostatic term (sic correction);[4,5] (ii) interpolating the DFT functional with the self-interaction free Hartree-Fock exchange energy (hybrid functionals);[6,7] and (iii) directly modifying the KS potential to make it reproduce essential features of exact exchange.[8–13] However, none of these schemes provide a general treatment of this error within an unaltered semilocal DFT framework. Another observation of the difficulty for XC functionals to deal with systems with electrons confined in space can be made in that functionals which are not specifically oriented toward quantum chemistry (e.g., by fitting to atoms and small molecules) often have trouble with such systems (see, e.g., Ref. 14). Connections have been made also between such errors and the self-interaction error.[15]

Rather than focusing on the surplus term from the Hartree energy, the present work takes a very density-functional centric view of the error in systems with localized states. We use a harmonic-oscillator (HO) model to quantify the inability of current semilocal XC functionals to reproduce the exact exchange energy in a system confined in one of its three dimensions, which thus implicitly includes the functionals' lack of ability to cancel the self-interaction error in this situation. The magnitudes of the errors are connected to a measure of how confined the system is, and based on this we conclude that spatial regions in a system can be classified as more or less dominated by, as we name it, "confinement physics." The motivation, discussion, and quantification of this concept are main points of this paper. Most importantly, the existence of a confinement physics error inherent to specific spatial regions in a system enables a parallel with how the implicit surface error[16–18] previously have been successfully handled through correction schemes[17–19] and in the construction of the Armiento-Mattsson 2005 (AM05) functional.[20] Hence, our results open for a similar scheme for correcting the errors for systems with localized electron states.

The rest of the paper is organized as follows: in Sec. II we give some background on the XC functionals used in this work and clarify the parallel between how prior work has treated the implicit surface region error and how the here relevant confinement physics error can be addressed. In Sec. III, we give the details of the HO model system used in our investigation. In Sec. IV, we study the effect of confinement on the electron density. In Sec. V, we make small perturbations around the HO model system to make sure our results in the foregoing section are universal, i.e., not unique for the highly symmetric HO model alone. In Sec. VI we study the effects of confinement on the exchange energy. In Sec. VII, we compare the performance of several currently used functionals for the exchange energy per particle and total exchange energy of the HO gas, and show that none of them

adequately handles strongly confined HO systems. Section VIII presents our summary and conclusions.

II. EXCHANGE-CORRELATION FUNCTIONALS AND THE SUBSYSTEM FUNCTIONAL SCHEME

Massive efforts have been devoted to the search for well performing functionals. By assuming that the XC energy depends solely on the magnitude of the electron density in each point in space, the local-density approximation (LDA) was derived from the uniform electron-gas (UEG) model. Thereafter, several competing schemes have been proposed to construct effective density functionals. Two of them will be discussed in the following, the Jacob's ladder scheme and the subsystem functional scheme.

The Jacob's ladder scheme suggested by Perdew *et al.*[21] is to include additional local ingredients at each higher rung of the ladder, and thereby being able to satisfy more limits and other constraints that the exact exchange and correlation functionals have been proven to fulfill. This scheme has led to many functionals of widespread use today, such as the functional of Perdew, Burke, and Ernzerhof (PBE),[22] its revised version called PBEsol,[23] and the functional of Tao, Perdew, Staroverov, and Scuseria (TPSS).[24]

The subsystem functional scheme is another route for functional development, which originates from a very different viewpoint initiated by Kohn, Mattsson, and Armiento.[16,25] This approach is based on the observation of the "nearsightedness" of electrons.[26] The total XC energy can be expressed as an integral over local contributions from each point in space,

$$E_{\mathrm{XC}} = \int_V n(\mathbf{r})\epsilon_{\mathrm{XC}}(\mathbf{r};[n])dV. \tag{1}$$

The idea of the subsystem functional scheme is to divide the entire integration space V into several contiguous subsystems, V_j. In each subsystem, the characteristic physics is described by different density functionals, XC energy per particle $\epsilon_{\mathrm{XC}}^j(\mathbf{r};[n])$, which is designed based on a characteristic model system. Then the total XC energy is evaluated by summing over these subsystems,

$$E_{\mathrm{XC}} = \sum_{j=1}^{N} \int_{V_j} n(\mathbf{r})\epsilon_{\mathrm{XC}}^j(\mathbf{r};[n])dV. \tag{2}$$

LDA can be considered as the simplest subsystem functional, containing only one model system, the UEG. After 40 years of its invention, surprisingly LDA is still widely in use and performs very well in numerous applications. The good performance of LDA stems from the *compatibility* of its exchange and correlation energies as they are derived based on one single model, the UEG, which enables errors in the exchange and correlation to cancel each other.[27]

The subsystem functional scheme makes use of this kind of compatibility since each subsystem functional is developed based on a single model system. The AM05 functional[20] took a step beyond LDA by including more types of physics using two different model systems: the UEG and the Airy gas (AG) model.[16] While the UEG is based on a constant effective potential and gives a good description of the physics in the interior regions of solid state materials, the AG uses a strictly linear potential that crosses the chemical potential, mimicking situations near surfaces and other regions with rapidly varying electron density. We refer to such regions as "edges."

For practical purposes, it is necessary to have a built-in mechanism to automatically separate the system into subregions and apply the specialized functionals. Based on the local character of the density, AM05 incorporated such a mechanism by introducing an interpolation index $X(s)$, where $s=\frac{\nabla n}{2(3\pi^2)^{1/3}n^{4/3}}$ is the dimensionless gradient characterizing the local variations in the density. Thus, a general functional is constructed in the following form:

$$\epsilon_{\mathrm{XC}}^{\mathrm{AM05}}(\mathbf{r};[n]) = \epsilon_{\mathrm{XC}}^{interior}(n)X(s) + \epsilon_{\mathrm{XC}}^{edge}(n,s)[1-X(s)]. \tag{3}$$

The AM05 functional has been used for calculating various material properties of miscellaneous systems[28–31] and is proven to perform exceptionally well for solids and surfaces. However, the performance is not as good for systems of more localized characters due to the lack of description of confinement physics in the functional as we discussed in Sec. I. This limitation is also shared by all other semilocal functionals. It is highly appealing to have a general functional that includes all the ingredients of the interior physics, the edge physics, and the confinement physics, especially for solving problems involving systems that exhibit both extended and localized characters. The subsystem functional scheme suggests a feasible way to attain such a functional by following the same strategy used in building the AM05 functional:

$$\begin{aligned}\epsilon_{\mathrm{XC}}(\mathbf{r};[n]) = {} & \epsilon_{\mathrm{XC}}^{interior}(n)X_1[n](1-X_2[n]) \\ & + \epsilon_{\mathrm{XC}}^{edge}(n,s)(1-X_1[n])(1-X_2[n]) \\ & + \epsilon_{\mathrm{XC}}^{confined}[n](1-X_1[n])X_2[n],\end{aligned} \tag{4}$$

where $X_1[n]$ and $X_2[n]$ are the interpolation indices to help determining how different characteristic physics are mixed at a specific point.

The first step for constructing this functional is to parametrize the subsystem functional $\epsilon_{\mathrm{XC}}^{confined}[n]$ from a model system containing the confinement physics. The Mathieu gas (MG) model, based on a sinusoidal effective potential, has been proposed as a possible candidate for describing the confinement physics.[25] Its highly tunable parameter space has a wide spectrum of physical ingredients, which naturally evolve from the slowly varying interior physics to the targeted confinement physics. However, it is a very difficult task to parametrize the MG into a simple and useful functional owing to the nonanalyticity of the conventional exchange energy per particle expansion in the slowly varying limit,[25] and its relatively complicated parameter space with two degrees of freedom. Depending on the relative position of the chemical potential, the MG reaches two limits in the parameter space. One is the slowly varying limit, resembling the UEG, when the chemical potential is far above the effec-

tive potential. The other one is the HO limit as the chemical potential approaches the very bottom of the sinusoidal effective potential, the electrons are equivalent to being confined in harmonic-oscillator potential wells. Thus it is a natural line of logic to understand the confinement physics starting from the simpler HO model.

III. HARMONIC-OSCILLATOR MODEL

We consider a model system in which the noninteracting KS particles are moving in an effective potential that is not constrained in the x and y directions but restricted with a parabolic trap in z dimension. We will use the hartree unit system in the following unless otherwise indicated. We choose the conventionally used form of the HO potential

$$v_{eff}(z) = \frac{\omega^2}{2} z^2, \tag{5}$$

where ω represents the potential strength. Separating variables in the KS equation,

$$\left[-\frac{1}{2}\nabla^2 + v_{eff}(z) \right] \psi_\nu(\mathbf{r}) = E_\nu \psi_\nu(\mathbf{r}), \tag{6}$$

the normalized eigenfunctions are expressed as

$$\psi_\nu(\mathbf{r}) = \frac{1}{\sqrt{L_1 L_2}} e^{i(k_1 x + k_2 y)} \phi_j(z), \tag{7}$$

where $\nu \equiv (k_1, k_2, j)$, $k_i L_i = 2\pi m_i$ ($i=1$, 2, m_i is an integer), and $L_1 L_2$ is the area in x-y dimensions, which will approach infinity. $\phi_j(z)$ is the wave function for the one-dimensional KS equation,

$$\left(-\frac{1}{2}\frac{d^2}{dz^2} + \frac{\omega^2}{2} z^2 - \epsilon_j \right) \phi_j(z) = 0. \tag{8}$$

Scaling the coordinate z with a constant length $l = \sqrt{\frac{1}{\omega}}$, we obtain a dimensionless coordinate $\bar{z} = z/l$, with which we rewrite the KS equation and obtain

$$\left(\frac{d^2}{d\bar{z}^2} - \bar{z}^2 + 2l^2 \epsilon_j \right) \phi_j(z) = 0. \tag{9}$$

The normalized eigenfunctions and eigenenergies for the above differential equation take the following form:

$$\phi_j(z) = \left(\frac{1}{l\sqrt{\pi} 2^j j!} \right)^{1/2} \mathrm{H}_j(\bar{z}) e^{-\bar{z}^2/2}, \tag{10}$$

$$\epsilon_j = \frac{1}{l^2}(j + 1/2), \tag{11}$$

where $H_j(\bar{z})$ are the Hermite polynomials.

We let the chemical potential take the form $\mu = (\alpha + \frac{1}{2})\frac{1}{l^2}$, where we follow the same notation as in Ref. 25, that α is a real number, whose integer part $N = \lfloor \alpha \rfloor$ is the index of the highest level electrons can occupy in the z dimension, and the remainder $0 \le \alpha - N < 1$ is denoting the continuous bands in the x-y direction. The index α is quantifying the level of confinement. For a fixed μ, larger α leads to a wider opening of the parabolic potential (larger l), and therefore implies a less confined situation. This α-dependent confinement will be further discussed in the rest of the paper.

The density of the HO gas is

$$n(z) = 2\sum_{j=0}^{N} \phi_j^2(z) w_j, \quad w_j = \frac{1}{2\pi}(\mu - \epsilon_j), \tag{12}$$

where the factor of 2 accounts for the spins. Inserting the wave functions of the HO gas, Eq. (10), we can derive the (dimensionless) density,

$$[l^3 n(\bar{z})] = \frac{1}{\pi^{3/2}} \sum_{j=0}^{N} \frac{1}{2^j j!} H_j^2(\bar{z}) e^{-\bar{z}^2} (\alpha - j). \tag{13}$$

As derived in Ref. 16, when electrons can move freely in the x and y dimensions, the conventional exchange energy per particle ϵ_x^{conv} is

$$\epsilon_x^{conv}(\mathbf{r}) = -\frac{1}{2\pi n(z)} \int dz' \sum_j \sum_{j'} \phi_j(z)\phi_j(z')\phi_{j'}(z)\phi_{j'}(z') \times (\Delta z)^{-3} g(k_j \Delta z, k_{j'} \Delta z), \tag{14}$$

where $\Delta z = |z - z'|$. k_j is the maximum transverse wave number associated with $\phi_j(z)$: $k_j = \sqrt{2(\mu - \epsilon_j)}$. $g(s,s')$ is a universal function defined as

$$g(s,s') = ss' \int_0^\infty dt \frac{J_1(st) J_1(s't)}{t\sqrt{1+t^2}}, \tag{15}$$

where $J_1(x)$ is the Bessel function of the first kind.

Substituting $\phi_j(z)$ with the HO wave function, Eq. (10), the conventional (dimensionless) exchange energy per particle for the HO gas is obtained

$$[l\epsilon_x^{conv}(\bar{z})] = -\frac{1}{2\pi^2 [l^3 n(\bar{z})]} \int d\bar{z}' \sum_{j=0}^{N} \sum_{j'=0}^{N} \frac{1}{2^j j! 2^{j'} j'!} \times H_j(\bar{z}) H_j(\bar{z}') H_{j'}(\bar{z}) H_{j'}(\bar{z}') e^{-(\bar{z}^2 + \bar{z}'^2)} (\Delta\bar{z})^{-3} \times g[\sqrt{2(\alpha - j)}\Delta\bar{z}, \sqrt{2(\alpha - j')}\Delta\bar{z}]. \tag{16}$$

With the above dimensionless representation, HO gases with different potential strength ω now fall into one representation in which the physical quantities like the density n and exchange energy per particle ϵ_x will depend only on where the point of interest is in the HO gas as denoted by $\bar{z}$ and how many quantum energy levels are occupied as represented by α.

IV. POTENTIAL→DENSITY MAPPINGS

In Thomas-Fermi theory,[32,33] an approximation for the true density of an electron gas is obtained through a mapping from the effective potential ($V \to n$). By regarding a specific point in the potential as if it is in a uniform electron-gas potential with the same magnitude of difference between the chemical and effective potentials, the mapped density reads

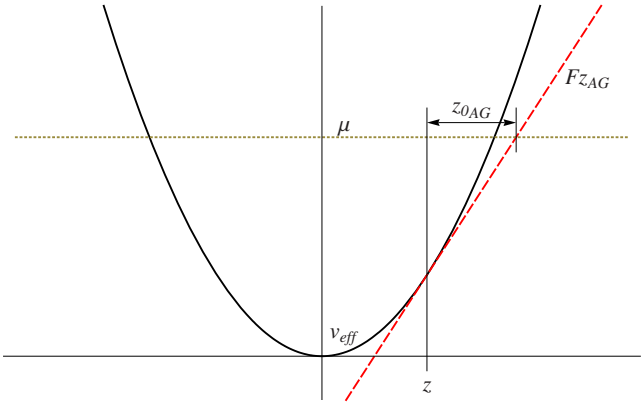

FIG. 1. (Color online) An illustration of the Airy gas-based $V \rightarrow n$ mapping applied to the HO gas.

$$n_{\mathrm{UEG}}^{V\rightarrow n}(\mathbf{r}) = \frac{1}{3\pi^2}\{2[\mu - v_{eff}(\mathbf{r})]\}^{3/2} \quad \mu > v_{eff}$$

$$= 0 \quad \mu < v_{eff}. \tag{17}$$

Applying the above mapping to the HO gas, the dimensionless density becomes

$$[l^3 n_{\mathrm{UEG}}^{V\rightarrow n}(\bar{z})] = \frac{l^3}{3\pi^2}(2\alpha + 1 - \bar{z}^2)^{3/2} \quad \bar{z}^2 < 2\alpha + 1$$

$$= 0 \quad \bar{z}^2 > 2\alpha + 1. \tag{18}$$

In Ref. 16, the density of the Airy gas and its approximation by the above UEG-based $V \rightarrow n$ mapping are compared. The density obtained by the UEG mapping is zero outside of the edge, where the exact AG solution shows nonzero electron densities. The UEG mapping also fails to reproduce the Friedel oscillations, a characteristic of the AG. Hence the characteristic properties of the edge physics are disclosed by comparing the UEG derived density and the true density. Our objective in this section is to reveal the confinement physics in the HO gas system by applying two types of $V \rightarrow n$ mappings based, respectively, on the UEG, as shown above, and the AG, which we will introduce in the following.

As illustrated in Fig. 1, we propose an alternative $V \rightarrow n$ mapping based on the AG instead of the UEG. That is, depending on the values of (1) the difference between the chemical and effective potentials, and (2) the gradient of the potential, we determine a value for the density in a point from the Airy gas density.

The AG is defined from a linear potential $v_{eff} = Fz$. Similarly to the HO gas, a dimensionless representation also exists for the AG by employing a scaling length $l_{\mathrm{AG}} = (2F)^{-1/3}$. Thus, following the derivation in Ref. 16, and defining the dimensionless coordinate $\bar{z}_{\mathrm{AG}} = z/l_{\mathrm{AG}}$, the density of the AG can be expressed in an analytical form based on the Airy function $\mathrm{Ai}(\bar{z}_{\mathrm{AG}})$ and its derivative:

$$n_{\mathrm{AG}}(\bar{z}_{\mathrm{AG}}) = \frac{1}{l_{\mathrm{AG}}^3} n_{0\mathrm{AG}}(\bar{z}_{\mathrm{AG}}),$$

$$n_{0\mathrm{AG}}(\bar{z}_{\mathrm{AG}}) = [\bar{z}_{\mathrm{AG}}^2 \mathrm{Ai}^2(\bar{z}_{\mathrm{AG}}) - \bar{z}_{\mathrm{AG}} \mathrm{Ai}'^2(\bar{z}_{\mathrm{AG}}) - \mathrm{Ai}(\bar{z}_{\mathrm{AG}})\mathrm{Ai}'(\bar{z}_{\mathrm{AG}})/2]/(3\pi). \tag{19}$$

In order to perform the AG-based mapping, we need two equations to determine the values of F and $z_{0\mathrm{AG}}$,

$$F = v'_{eff}(z), \tag{20}$$

$$Fz_{0\mathrm{AG}} = \mu - v_{eff}(z). \tag{21}$$

This gives a local scaling length of the Airy gas

$$l_{\mathrm{AG}}(z) = \left(\frac{1}{2F}\right)^{1/3} = \left[\frac{1}{2v'_{eff}(z)}\right]^{1/3} \tag{22}$$

and the $V \rightarrow n$ mapping based on the AG at the point z is

$$n_{\mathrm{AG}}^{V\rightarrow n}(z) = \frac{1}{l_{\mathrm{AG}}^3(z)} n_{0\mathrm{AG}}[z_{0\mathrm{AG}}(z)/l_{\mathrm{AG}}(z)]. \tag{23}$$

Applying this to the harmonic-oscillator effective potential in Eq. (5), gives

$$l_{\mathrm{AG}}(z) = l\left(\frac{1}{2\bar{z}}\right)^{1/3}, \tag{24}$$

$$z_{0\mathrm{AG}} = l\frac{2\alpha + 1 - \bar{z}^2}{2\bar{z}}, \tag{25}$$

and finally

$$[l^3 n_{\mathrm{AG}}^{V\rightarrow n}(\bar{z})] = (2\bar{z}) n_{0\mathrm{AG}}\left[\frac{(2\alpha + 1) - \bar{z}^2}{(2\bar{z})^{2/3}}\right]. \tag{26}$$

We perform the UEG and AG-based $V \rightarrow n$ mappings on the HO gas with occupation number $\alpha = 0.23$ [Fig. 2(a)] and 3.87 [Fig. 2(b)] by employing Eqs. (18) and (26). For the relatively high occupation number of $\alpha = 3.87$, both the UEG- and AG-based mappings produce good approximations to the exact HO gas density except for that the UEG mapping cannot describe the nonvanishing density outside of the edge. In the case of $\alpha = 0.23$, there are less electrons in the HO system than both the UEG and AG mappings have expected. This is because in both cases the system is anticipated to be infinite with continuous energy levels from all three dimensions that can be occupied from the bottom of the potential. However, the real situation is that the HO system is confined in the z dimension, which takes away the continuum spectrum in this dimension so that we only have a two-dimensional (2D) energy-level continuum that can be populated with electrons, therefore, the density becomes lower than if we had not confined the system.

V. PERTURBED HO GAS

The HO electron gas is one of the few inhomogeneous interacting many-body systems whose dynamic properties can be solved exactly. Kohn's theorem,[34] and its generalizations,[34–36] "*in the ideal parabolic well the optical absorption spectrum* [of the electron gas] *is independent of the electron-electron interaction, and also independent of the*

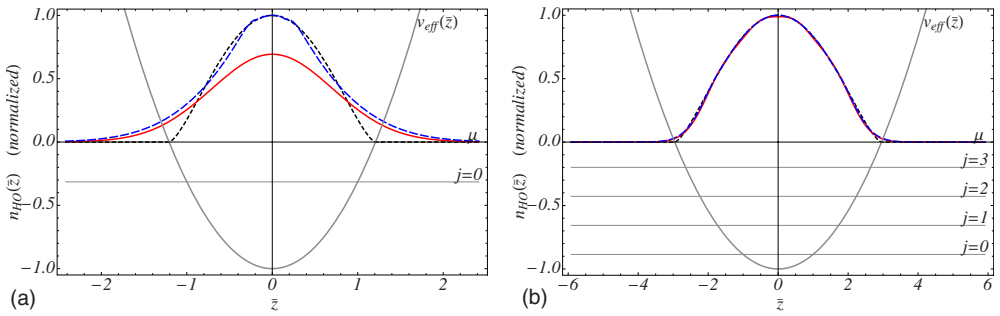

FIG. 2. (Color online) The normalized density of the HO gas (red solid) and the approximate density obtained with the $V\rightarrow n$ mapping based on the UEG (dotted; black online) and the AG (dashed; blue online), see text. Occupancy with (a) $\alpha=0.23$ and (b) $\alpha=3.87$ are shown. Shown is also the HO potential used in the mapping and the corresponding discrete energy levels ϵ_j from Eq. (11). Here the x axis of the plot represents the chemical potential μ. Note that the UEG-based $V\rightarrow n$ mapping gives zero density outside of the edge.

number of electrons in the well." Slight perturbations will break this symmetry and may result in drastic variations in the electron-gas properties. In this paper, only the ground-state properties of the HO gas are studied but it is still essential to examine whether the electron density will change discontinuously as the potential of HO gas is distorted slightly. As discussed above, the HO is one of the limits of the MG [see Fig. 3(a)]. In the following, we will answer this question by investigating the density variations as the external potential deviates from the HO to the MG.

The effective potential of the MG is described by a two-parameter model,

$$v_{eff}^{\mathrm{MG}}(z)=\lambda[1-\cos(pz)]. \tag{27}$$

Following the notations in Ref. 25, the model parameters can be written in dimensionless form $\bar{\lambda}=\lambda/\mu$ and $\bar{p}=p/(2k_{F,u})$ by considering the chemical potential μ. Here $k_{F,u}^2=2\mu$ is the Fermi wave vector of a uniform electron gas with chemical potential μ. The coordinate of the system is also represented in dimensionless form, $\bar{z}_{\mathrm{MG}}=k_{F,u}z$.

In the limit $\bar{\lambda}=\lambda/\mu\rightarrow\infty$, the effective potential of the MG, Eq. (27), can be expanded around $z=0$ into a HO form

$$v_{eff}^{\mathrm{MG}}(z)=\frac{\lambda p^2}{2}z^2+O(z^4). \tag{28}$$

Equation (30) in Ref. 25 gives a relation between the MG parameters and the HO occupation number α when the MG is approaching the HO limit,

$$\alpha=\frac{1}{2\sqrt{2\bar{\lambda}\bar{p}^2}}-\frac{1}{2}. \tag{29}$$

Also considering that λp^2 is equivalent to ω^2 in the HO gas, and with some algebra, the mapping from the MG to the HO system can be straightforwardly found to be

$$\bar{z}_{\mathrm{HO}}=\bar{z}_{\mathrm{MG}}\frac{1}{\sqrt{2\alpha+1}},$$

$$[l^3 n_{\mathrm{HO}}(\bar{z}_{\mathrm{HO}})]=\frac{n_{\mathrm{MG}}(\bar{z}_{\mathrm{MG}})}{n_u}\frac{(2\alpha+1)^{3/2}}{3\pi^2}, \tag{30}$$

where $\frac{n_{\mathrm{MG}}(\bar{z}_{\mathrm{MG}})}{n_u}$ is calculated according to Eq. (B2) in Ref. 25. $1/2\bar{\lambda}=\mu/2\lambda$ characterizes the relative position of the chemical potential compared to the height of the effective potential of the MG, 2λ, and determines the perturbation extent of the MG potential from the HO.

In Fig. 3(b), we show the density of the HO gas with $\alpha=3.87$ and several MGs who have the same occupation number α as the HO but with different $\bar{\lambda}$. The parameter $\bar{p}$ of these MGs is obtained through Eq. (29). When the relative height of the chemical potential is 1/100 of the MG potential, $\bar{\lambda}=50$, electrons cannot see the finite barrier of the MG potential, hence they are equivalent to being in an infinitely high HO potential, and there are no difference of the densities between the MG and the HO systems. When we increase the relative height of the chemical potential to 1/4 ($\bar{\lambda}=2$), and 1/2 ($\bar{\lambda}=1$) of the MG effective potential, the densities start to spread out over the edge by electrons tunneling through the finite barrier of the MG potential but the perturbation compared to the HO density is still limited, especially in the center of the well. The continuous changes in the electron density as the potential is perturbed from the HO to the MG imply that the HO gas is not a special system in our case and can generally describe the confinement physics.

VI. DENSITY→EXCHANGE ENERGY PER PARTICLE MAPPING

Recently Engel and Schmid[37] have shown that, by combining the exact exchange and LDA correlation, DFT can

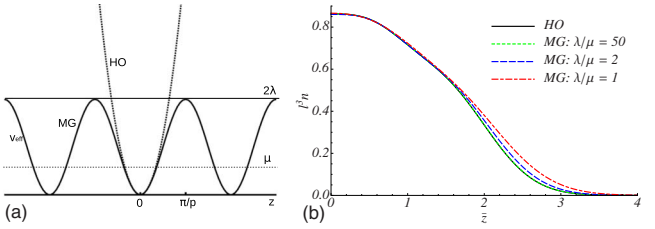

FIG. 3. (Color online) (a) The Mathieu gas potential and its HO limit. (b) The dimensionless density of the HO gas with $\alpha=3.87$ and mappings from the Mathieu gas with $\bar{\lambda}=50$, $\bar{\lambda}=2$, and $\bar{\lambda}=1$.

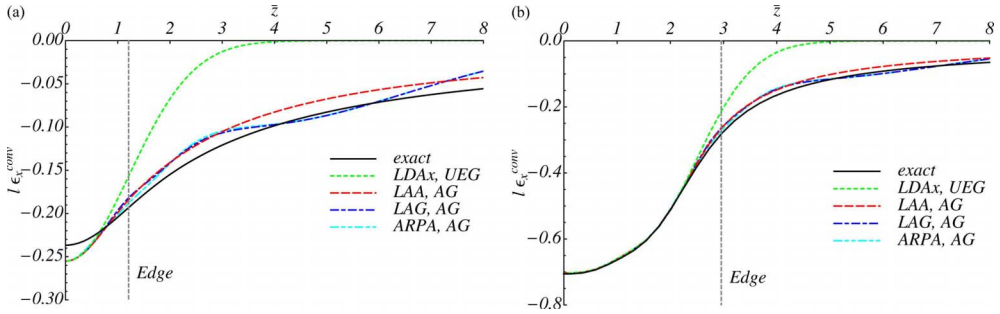

FIG. 4. (Color online) The $n \rightarrow \epsilon_x$ mappings based on the UEG or AG models are applied on the HO electron gases and compared with the exact ϵ_x value. The dimensionless exchange energy per particle ($l\epsilon_x^{conv}$) is plotted as function of the scaled length $\bar{z}$, for (a) $\alpha=0.23$ and (b) $\alpha=3.87$. The exchange parametrization and its corresponding model system are listed in the legend.

correctly yield the insulating ground states for transition-metal monoxides while LDA and generalized gradient approximation (GGA) exchange normally give incorrect results of ground states with metallic character. This implies that a major part of the confinement physics is incorporated in the exchange part of the XC energy. This is also in line with the analogy to the self-interaction error in Hartree-Fock, where the exchange term cancels all self-interaction. In the following, we will show that, by performing a density-to-exchange energy per particle ($n \rightarrow \epsilon_x$) mapping based on the UEG and AG models for the HO gas and comparing with the true ϵ_x, the concealed confinement physics in the HO gas can be identified.

The LDA exchange parametrization can be considered as an $n \rightarrow \epsilon_x$ mapping based on the UEG, and therefore provides a good description of the interior physics. On the other hand, the AG-based mapping describes the edge physics, and there are several different available parametrizations, all of which use a GGA-type representation $\epsilon_x(n,s)=\epsilon_x^{\mathrm{LDA}}(n)F_x(s)$, where F_x is the refinement factor characterizing the dependence on the dimensionless gradient s. The local Airy gas (LAG) (Ref. 38) exchange parametrization introduced by Vitos *et al.* employs a modified Becke form to fit the exact AG exchange, and produces very good agreements over the range of $0<s<20$. The local Airy approximation (LAA) (Ref. 20) used in the AM05 functional is built by exploring the asymptotic behavior of the exact exchange of the AG, and hence is accurate also in the region far outside of the surface where s is large. Instead of placing the hard wall infinitely far away and occupying an infinite number of orbitals as in the AG modeling used in the LAG and LAA, Perdew and co-workers[39] chose an alternative AG model with a finite number of orbitals occupied, and parametrized it using an extension of the LAG form. We will use ARPA denoting this parametrization since it is developed for the construction of the airy gas-based random phase approximation (ARPA) functional in Ref. 39.

In Fig. 4, we compare the exact dimensionless exchange energy per particle, $l\epsilon_x$, as calculated in Eq. (16) for the HO gas, and the mapped values from the UEG and the AG models using the exact densities of the HO gas, as calculated from Eq. (13). In panel (a), we show a strongly confined system, with a low occupation number $\alpha=0.23$. The UEG-based mapping gives entirely different values of $l\epsilon_x$ compared to the exact ones. In the central region of the potential well ($\bar{z}\approx 0$), the UEG mapping overestimate the exchange energy per particle for the confined HO gas while beyond the edge ($|\bar{z}|>\sqrt{2\alpha+1}$), it approaches zero much faster than the exact HO gas does. The AG-based exchange parametrizations account for the surface effect, thus give results that agree better with the exact values, but they still overestimate the $l\epsilon_x$ values in the central region of the potential well, where the variation in density is small and they approach the UEG limit. For $\bar{z}<2$, the scaled gradient $s<20$ and all the AG-based exchange parametrizations give consistent values, indicating the physics a single edge gives. Far outside of the edge, however, s is much larger than 20, so the LAG and ARPA results are not reliable. LAA keeps the good asymptotic properties of the Airy gas in this region and should be used for representing the exact AG. We see that LAA produces a curve with almost the same shape as the exact curve but shifted closer to the x axis with a constant quantity. Overall, UEG- and AG-based functionals overestimate $l\epsilon_x$ inside of the potential well and underestimate it on the surface. For all $\alpha<0.84$, this overestimation of $l\epsilon_x$ in the center of the potential well is found.

In panel (b), the same comparison is performed for the HO gas with $\alpha=3.87$, a system with more occupied bands. We see all the AG-based exchange parametrizations now agree very well with the exact HO gas results, suggesting the confinement physics is less essential in this case. The LDA exchange parametrization still underestimates the magnitude of exchange in the edge region, as expected.

The UEG- and AG-based $n \rightarrow \epsilon_x$ mappings reveal the confinement characteristics of the HO gas, as do the $V \rightarrow n$ mappings in Fig. 2. By comparing Figs. 2 and 4, we see consistent information is exposed by these two mappings. For systems with large α, both AG-based mappings agree well with the exact density/exchange energy, indicating the dominance of the edge physics and the lack of confinement physics in such systems. For small α systems, both mappings not only deviate badly from the exact values, as a strong indication of the presence of the confinement physics, but also underestimate values of the density/exchange energy in the central region of the potential well, suggesting a characteristic effect brought by the confinement.

VII. COMPARISON WITH EXCHANGE FUNCTIONALS

The formulation of the total XC energy, Eq. (1), leaves us a freedom of choice for the XC energy per particle,

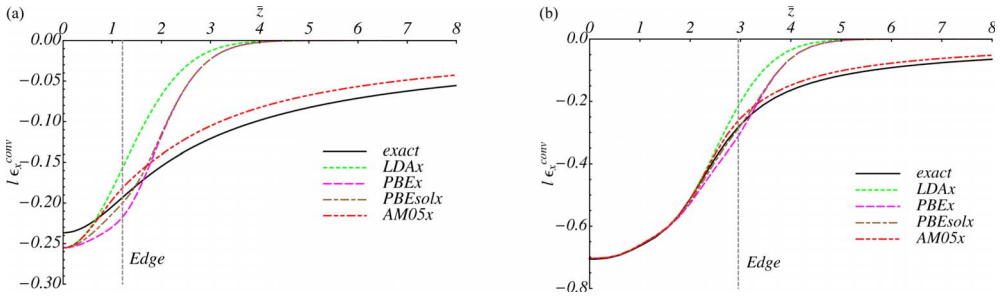

FIG. 5. (Color online) The dimensionless exchange energy per particle ($l\epsilon_x^{conv}$) as function of scaled length $\bar{z}$ for electrons in an HO effective potential with (a) α=0.23 and (b) α=3.87. The exactly calculated values are compared with those from LDA, AM05, PBE, and PBEsol functionals. Note that both the PBE and PBEsol exchanges are based on a different definition of exchange energy per particle than those in Fig. 4 as discussed in the first paragraph of Sec. VII and, in more details, in Ref. 25.

$\epsilon_{XC}(\mathbf{r};[n])$. Let $f(\mathbf{r})$ be an arbitrary function that gives zero when integrated over V, then $\epsilon_{XC}(\mathbf{r};[n])$ and $\epsilon_{XC}(\mathbf{r};[n])+f(\mathbf{r})/n(\mathbf{r})$ are equivalently valid despite of considerable differences locally. In contrast to LDA and AM05, PBE and PBEsol use this freedom. Because of this, and since AM05 more heavily relies on the cancellation of errors due to compatibility between exchange and correlation, their exchange energy per particle are quite different, even though the functionals have shown similar performance.[40,41]

In Fig. 5(a), the dimensionless exchange energy per particle given by several popular functionals are compared with the exact values in the HO gas for a system with α=0.23. The AM05 exchange is an interpolation between the LDA and LAA parametrizations [see Eq. (3)] and shows a similar curve as the LAA. Instead of a long tail extending far outside of the edge as the exact results show, PBE and PBEsol quickly approach zero when going beyond the edge. It should be especially noted that although these two functionals fail to approximate the exact exchange per particle outside of the edge, inside of the potential well, PBE shows a very close similarity to the exact values except for a constant shift to the negative. We suspect this is an indication of the presence of confinement physics in PBE, as the PBE functional is known to be biased toward the description of small atomic and chemical systems, and should have considerable confinement physics built in. PBEsol is more similar to LDA since it restores the density gradient expansion for exchange.

In Fig. 5(b), again we show the comparison in a less confined system with α=3.87. Inside of the edge, we note that PBEsol more closely agrees with the exact results in the edge region than do PBE and AM05. Despite the differences between PBEsol and AM05 in Fig. 5(b), these two functionals often lead to similar results when combined with the correlation, as discussed in Ref. 40.

The interpolation index $X(s)$ in Eq. (3) is used to distinguish the bulk and edge regions of a system. Equation (3) implies that in the bulk part, the exchange of AM05 will be indistinguishable from LDA. AM05 starts to deviate from LDA only when approaching the edge region of the system. For the HO gas, we clearly see this trend in Fig. 5, where AM05 and LDA exchange are the same in the central part of the potential, and begin to show difference only at the crossover from the bulk to the edge.

Ultimately it is the total XC energy E_{XC} that determines the accuracy of the self consistent DFT calculations. As already mentioned in Sec. V, the exchange contains a major part of the confinement physics, and therefore in the following section we will focus on examining how accurately present functionals approximate E_x.

The (dimensionless) total exchange energy of the HO gas, (l^3E_x), depends on the occupation number α, and can be obtained by

$$[l^3E_x(\alpha)] = \int_{-\infty}^{\infty} [l^3 n(\bar{z},\alpha)][l\epsilon_x^{conv}(\bar{z},\alpha)]d\bar{z}. \tag{31}$$

In Fig. 6, we show the relative errors of the total exchange energy $\Delta E_x/E_x^{exact}=(E_x-E_x^{exact})/E_x^{exact}$ introduced by using different functional approximations. The E_x^{exact} is the exact value of the total exchange energy evaluated by inserting

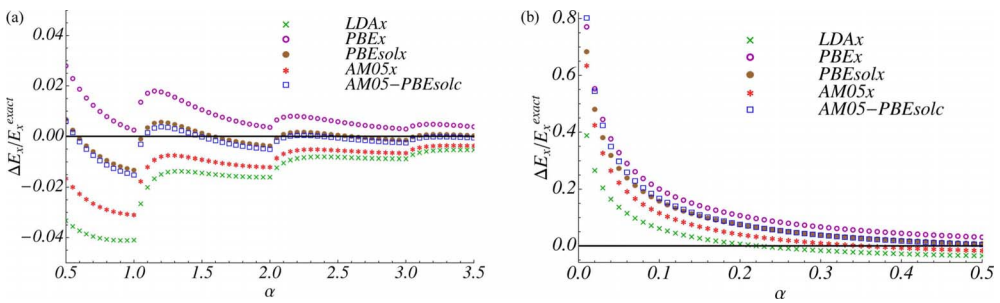

FIG. 6. (Color online) The relative errors of the total exchange energy $(E_x-E_x^{exact})/E_x^{exact}$ from different existing functionals versus occupancy α. The squares (blue online) are for $[(E_{XC}^{AM05}-E_c^{PBEsol})-E_x^{exact}]/E_x^{exact}$ to illustrate the compatibility of the AM05 exchange and correlation.

Eqs. (13) and (16) into Eq. (31), and E_x is obtained from the different approximate functionals.

In Fig. 6(a) we show systems with relatively large α. In this regime, the absolute value of relative errors from all the functionals is less than 4% and keep decreasing as α increases, which suggests a comparably good approximation by the present functionals due to the lack of confinement physics in these systems. When α is an integer, more subbands become available to be occupied, resulting in discontinuities in the plot. The relative errors of LDA are largest and always negative, which implies the underestimation of the exchange energy. In contrast, PBE always produces positive errors and overestimates E_x. The opposite corrections of the equilibrium properties by LDA and PBE have been observed in many applications, and it is also retained here in the approximation of the E_x in the HO gas with high α. Another interesting observation is that PBEsol generates the least relative errors with both positive and negative signs. The origin of this can be traced back to Fig. 5(b), where we see that PBEsol gives the closest approximation around the edge. AM05 is not producing the same small relative errors as PBEsol for the exchange. However, AM05 is constructed enforcing the cancellation of errors between the exchange and correlation in order to have an accurate full XC energy. By adding the exchange errors included in the AM05 correlation ($E_c^{\mathrm{AM05}}-E_c^{\mathrm{PBEsol}}$) to the AM05 exchange E_x^{AM05}, it gives as small relative errors as PBEsol [squares in Fig. 6(a) (blue online)]. This also shows that despite the difference in exchange and correlation, AM05 and PBEsol give the same total XC energy for these systems.

For highly confined systems, the situation is far from satisfactory, as seen in Fig. 6(b). Here systems with $0<\alpha<0.5$ are plotted, where only the first subband is filled. We note when α becomes very small, confinement physics plays an important role, thus all the functionals fail to produce a good approximation to E_x^{exact}. The relative errors can be as large as 70%, indicating a gross absence of the confinement physics in the present functionals. The positive relative errors for all functionals in small α systems imply that they all overestimate the absolute value of E_x. It is interesting to notice that the LDA functional actually provides the least errors compared to other functionals. Our investigation shows this is because the overestimation of the local contribution in Eq. (31), $(l^3n)(l\epsilon_x^{conv})$, in the interior region and the underestimation on the edge of the HO system cancel each other much better for LDA than for the other functionals.

The failure of conventional local and semilocal functionals when applied to quasi-two-dimensional systems have been extensively discussed in previous works in the context of "dimensional crossover,"[42–46] which is the situation when a three-dimensional (3D) electron gas is approaching the 2D limit. It is shown that all the semilocal functionals tend to overestimate the XC energy when one dimension of the electron gas is compressed to infinitesimal, which is consistent with what we have found in the present study. However, it is not our purpose in this paper to review this existing knowledge. Instead, by identifying that the HO gas contains the missing ingredient of the confinement physics, we pave the way for future work of constructing a compatible subsystem functional that incorporates this confinement physics. In our study we have considered the real situation that all the electron subbands are available to be occupied while in the previous work of Refs. 47 and 48 only the lowest subband is allowed to be populated. We thus probe the full range of quasi-2D systems between the 2D and 3D limits.

We also note that Constantin proposed a simple semilocal functional form, named GGA+2D, in Eq. (18) of Ref. 45, to improve the behavior of the semilocal functional in the quasi-2D region. The GGA+2D functional recovers the LDA result in the region where s is small. In the central part of the HO gas, the scaled density gradient s is approximately 0, and GGA+2D will give the same result as LDA. However, as already shown in Fig. 4, LDA does not approximate the exact result well in this part of the HO, which implies that GGA+2D is not a suitable choice for approximating the ϵ_x of the HO gas.

VIII. CONCLUSION

In this paper, we put forward the concept of *confinement physics*, a vital ingredient in many real systems when electrons are strongly localized in space, but which is largely absent in present density functionals. As a step toward the construction of a generic density functional that incorporates the missing ingredient of confinement physics within the subsystem functional scheme, we study a quasi-two-dimensional electron-gas model system confined by a HO potential.

We employ both the potential $\rightarrow$ density and the density $\rightarrow$ exchange mappings based on the UEG and AG models on the HO gas, and compare with the exact solutions. The UEG- and AG-based mappings represent the physical characters when electrons are in the interior and surface regions, and hence their differences from the exact HO results uncover the presence of the confinement physics. It is shown that the amount of confinement physics in the HO gas depends on the occupation number α. When α is large, more quantized levels are populated and the AG-based mappings are very close to the exact results, indicating a small portion of confinement character. When α is less than 1, only the lowest subband is populated, and the exactly determined density and exchange energy of the HO gas are substantially different than all the mappings, indicating the dominance of the confinement physics. The above observations are consistent for both the potential $\rightarrow$ density and the density $\rightarrow$ exchange mappings. In order to remove doubts about the specificity of the HO gas as shown in many previous studies, we examine the ground-state density when the potential is perturbed from the HO to the MG, and no discontinuous changes have been found, which confirms that the HO is a suitable system to describe the general confinement physics.

In the last part of the paper, we compare the total exchange energy E_x of the HO gas with several approximations by conventional LDA and GGA functionals. All of them overestimate E_x in strongly confined situations, which clearly illustrates deficiency of the description of confinement physics in currently used functionals.

A natural solution to the problem is using orbital-dependent exchange functionals, with the necessary tradeoff of much higher computational expenses. Our aim is to construct the simplest possible functional useful for calculations that are as computationally demanding as those correctly performed with commonly used GGA-type functionals. The subsystem functional scheme has been very successful in dealing with the surface physics in the construction of the AM05 functional. The same strategy can be applied for building a generic functional that also incorporates the confinement physics. The HO gas carries the essential confinement characters and is a suitable model system to build upon. A good parametrization of the HO gas exchange-correlation energy and a suitable choice of the interpolation index in Eq. (4) will hopefully lead to an accurate functional that includes all these important physical characters.

ACKNOWLEDGMENTS

We thank W. Kohn and R. J. Magyar for valuable discussions. This work was supported by the Laboratory Directed Research and Development Program. Sandia National Laboratories is a multiprogram laboratory operated by Sandia Corporation, a wholly owned subsidiary of Lockheed Martin Company, for the U.S. Department of Energy's National Nuclear Security Administration under Contract No. DE-AC04-94AL85000.

*fhao@sandia.gov
†armiento@mit.edu
‡aematts@sandia.gov

[1] P. Hohenberg and W. Kohn, Phys. Rev. **136**, B864 (1964).
[2] W. Kohn and L. J. Sham, Phys. Rev. **140**, A1133 (1965).
[3] F. Zhou, M. Cococcioni, C. A. Marianetti, D. Morgan, and G. Ceder, Phys. Rev. B **70**, 235121 (2004).
[4] J. Perdew, Chem. Phys. Lett. **64**, 127 (1979).
[5] J. P. Perdew and A. Zunger, Phys. Rev. B **23**, 5048 (1981).
[6] A. D. Becke, J. Chem. Phys. **98**, 5648 (1993).
[7] J. P. Perdew, M. Ernzerhof, and K. Burke, J. Chem. Phys. **105**, 9982 (1996).
[8] M. K. Harbola and V. Sahni, Phys. Rev. Lett. **62**, 489 (1989).
[9] O. Gritsenko, R. van Leeuwen, E. van Lenthe, and E. J. Baerends, Phys. Rev. A **51**, 1944 (1995).
[10] A. D. Becke and E. R. Johnson, J. Chem. Phys. **124**, 221101 (2006).
[11] N. Umezawa, Phys. Rev. A **74**, 032505 (2006).
[12] R. Armiento, S. Kümmel, and T. Körzdörfer, Phys. Rev. B **77**, 165106 (2008).
[13] E. Räsänen, S. Pittalis, and C. R. Proetto, J. Chem. Phys. **132**, 044112 (2010).
[14] S. Kurth, J. P. Perdew, and P. Blaha, Int. J. Quantum Chem. **75**, 889 (1999).
[15] Y. Zhang and W. Yang, J. Chem. Phys. **109**, 2604 (1998).
[16] W. Kohn and A. E. Mattsson, Phys. Rev. Lett. **81**, 3487 (1998).
[17] K. Carling, G. Wahnström, T. R. Mattsson, A. E. Mattsson, N. Sandberg, and G. Grimvall, Phys. Rev. Lett. **85**, 3862 (2000).
[18] A. E. Mattsson, R. R. Wixom, and R. Armiento, Phys. Rev. B **77**, 155211 (2008).
[19] A. E. Mattsson, R. Armiento, P. A. Schultz, and T. R. Mattsson, Phys. Rev. B **73**, 195123 (2006).
[20] R. Armiento and A. E. Mattsson, Phys. Rev. B **72**, 085108 (2005).
[21] J. P. Perdew, A. Ruzsinszky, J. Tao, V. N. Staroverov, G. E. Scuseria, and G. Csonka, J. Chem. Phys. **123**, 062201 (2005).
[22] J. P. Perdew, K. Burke, and M. Ernzerhof, Phys. Rev. Lett. **77**, 3865 (1996).
[23] J. P. Perdew, A. Ruzsinszky, G. I. Csonka, O. A. Vydrov, G. E. Scuseria, L. A. Constantin, X. Zhou, and K. Burke, Phys. Rev. Lett. **100**, 136406 (2008).
[24] J. Tao, J. P. Perdew, V. N. Staroverov, and G. E. Scuseria, Phys. Rev. Lett. **91**, 146401 (2003).
[25] R. Armiento and A. E. Mattsson, Phys. Rev. B **66**, 165117 (2002).
[26] W. Kohn, Phys. Rev. Lett. **76**, 3168 (1996).
[27] A. E. Mattsson and R. Armiento, Int. J. Quantum Chem. **110**, 2274 (2010).
[28] A. E. Mattsson, R. Armiento, J. Paier, G. Kresse, J. M. Willsand, and T. R. Mattsson, J. Chem. Phys. **128**, 084714 (2008).
[29] A. E. Mattsson and T. R. Mattsson, J. Chem. Theory Comput. **5**, 887 (2009).
[30] R. P. Muller, A. E. Mattsson, and C. L. Janssen, J. Comput. Chem. **31**, 1860 (2010).
[31] M. D. Knudson and M. P. Desjarlais, Phys. Rev. Lett. **103**, 225501 (2009).
[32] L. H. Thomas, Proc. Cambridge Philos. Soc. **23**, 542 (1927).
[33] E. Fermi, Rend. Accad. Naz. Lincei **6**, 602 (1927).
[34] W. Kohn, Phys. Rev. **123**, 1242 (1961).
[35] L. Brey, N. F. Johnson, and B. I. Halperin, Phys. Rev. B **40**, 10647 (1989).
[36] J. F. Dobson, Phys. Rev. Lett. **73**, 2244 (1994).
[37] E. Engel and R. N. Schmid, Phys. Rev. Lett. **103**, 036404 (2009).
[38] L. Vitos, B. Johansson, J. Kollar, and H. L. Skriver, Phys. Rev. B **62**, 10046 (2000).
[39] L. A. Constantin, A. Ruzsinszky, and J. P. Perdew, Phys. Rev. B **80**, 035125 (2009).
[40] A. E. Mattsson, R. Armiento, and T. R. Mattsson, Phys. Rev. Lett. **101**, 239701 (2008).
[41] P. Haas, F. Tran, P. Blaha, K. Schwarz, and R. Laskowski, Phys. Rev. B **80**, 195109 (2009).
[42] P. García-González, Phys. Rev. B **62**, 2321 (2000).
[43] P. García-González and R. W. Godby, Phys. Rev. Lett. **88**, 056406 (2002).
[44] L. A. Constantin, J. P. Perdew, and J. M. Pitarke, Phys. Rev. Lett. **101**, 016406 (2008).
[45] L. A. Constantin, Phys. Rev. B **78**, 155106 (2008).
[46] C. M. Horowitz, L. A. Constantin, C. R. Proetto, and J. M. Pitarke, Phys. Rev. B **80**, 235101 (2009).
[47] Y. H. Kim, I. H. Lee, S. Nagaraja, J. P. Leburton, R. Q. Hood, and R. M. Martin, Phys. Rev. B **61**, 5202 (2000).
[48] L. Pollack, and J. P. Perdew, J. Phys.: Condens. Matter **12**, 1239 (2000).